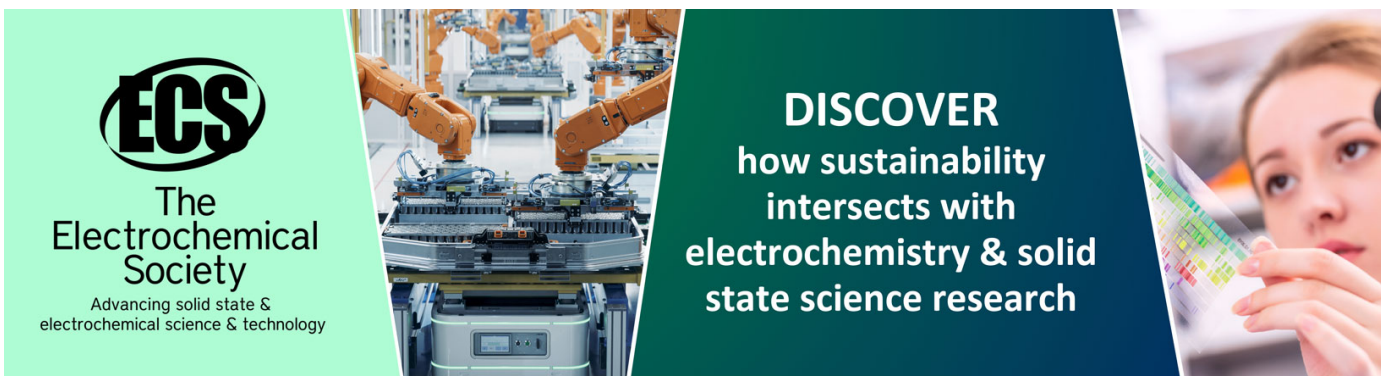**PAPER • OPEN ACCESS**

Heat fluxes distribution and uncertainty in low-Reynolds flow regimes inside a ribbed channel

To cite this article: L Vitali *et al* 2022 *J. Phys.: Conf. Ser.* **2177** 012037

View the article online for updates and enhancements.

Heat fluxes distribution and uncertainty in low-Reynolds flow regimes inside a ribbed channel

L Vitali, P Gramazio, D Fustinoni and A Niro

Politecnico di Milano, Department of Energy,
Campus Bovisa, Via Lambruschini 4, 20156 Milano, Italy

Corresponding author email: alfonso.niro@polimi.it

Abstract. Experimental studies on the local convective heat transfer enhancement induced by ribs in channels are generally carried out in steady state, by imposing a known heat flux on the ribbed surface and subsequently retrieving the convective heat flux by means of a local heat balance, i.e. by subtracting all the non-convective heat fluxes from the source term. Such heat fluxes are retrieved from temperature measurements by means of models, whose complexity can range from simple algebraic expressions to complex simulations. In this context, an experimental technique based on FEM simulations, a radiative model for semi-transparent enclosures, and a filtering technique to retrieve the heat fluxes across the plane of the heated surface has been developed and tested in a 1:10 AR channel, for Reynolds number ranging from 650 to 7500 and a flow of air. This paper presents a discussion on the heat flux distribution as a function of the Reynolds number for a streamwise-pointing chevron (V) rib configuration with 60° angle of attack, with P/e = 20, showing the increasing weight of non-convective heat dissipations as the Reynolds number decreases, and their effect on the uncertainty of the Nusselt number measurement.

1 Introduction

Heat transfer enhancement in closed channels by means of passive turbulators is still a topic actively researched, not only as this apparently simple technology has a wide range of applications, e.g. the cooling of turbine blades, of the first wall in fusion reactors and of photovoltaic modules, or the efficiency enhancement of solar air heaters, all characterized by different geometrical and fluid-dynamics parameters, but also because the overall heat transfer and pressure drop increment are underlain by complex fluid-dynamics phenomena, and the path towards a complete agreement between experimental and numerical analyses has yet to be fully traveled.

In scientific literature, the problem is usually analyzed from two main standpoints. The first is focused on measuring the overall heat transfer augmentation and pressure drop increment induced by specific configurations. Studies on single families of configurations are then compared in review articles, as done for example by Kumar and Kim [1], typically in terms of Nusselt number enhancement with respect to the smooth channel, i.e. Nu/Nu_0, and a thermohydraulic performance parameter η, often defined as a function of Nu and the friction factor f as follows:

$$\eta = (Nu/Nu_0)/(f/f_0)^{0.33} \tag{1}$$

The second approach consists of analyzing the local heat transfer augmentation given by simpler configurations, which are usually paired with CFD simulations for cross-validation purposes, see as example the work by Tanda and Satta on angled and intersecting ribs [2]. An analysis of the techniques employed for such experiments is beyond the scope of this work, but, with few notable exceptions, as the experiments carried out by Chung et al. [3] which exploit the heat-mass transfer analogy applied to the measurement of naphthalene sublimation, they are generally based on the retrieval of the temperature field on the surface under investigation by means of optical techniques, which is fed to appropriate thermal models to retrieve the desired convective heat flux.

The two approaches are complementary, and have been both used at the ThermALab Laboratory at Politecnico di Milano in a long-term study on heat transfer enhancement in closed channels, see for example [4] on the global approach. In particular, a channel with one heated wall has been built for improving the detail of the local convective heat transfer measurement, and a new analysis procedure has been developed by Gramazio, Vitali, Fustinoni and Niro, see [5] [6], in the effort to validate new CFD simulations by means of DNS. To this end, it is also important to study not only high-Reynolds regimes, i.e. Re > 10000, which are typical of applications like turbines and solar air heaters, but also low-Reynolds regimes, namely from 600 to 10000, as they can comprehend operational flow regimes of a wide array of compact heat exchangers. In this Reynolds range, there is a general lack of results in scientific literature, and the models required to retrieve the convective heat flux maps from temperature measurements should adequately take into account heat fluxes other than convective, namely conductive and radiative, as their relative contribution to the heat balance can be non-negligible.

Moreover, in many papers, see for example [7], [8], [9] and [10], uncertainties on the local Nusselt number are declared, usually based on analyses according to Moffat [12], which proposes an uncertainty estimation procedure for single-sample measurements, but the resulting values are hardly circumstantiated.

All that considered, the purpose of this paper is to analyze the local convective heat transfer results of a V-down rib configuration, in particular concerning the minimum uncertainty of the Nusselt number and the heat flux relative contribution to the total energy balance, highlighting the difference between high- and low- Reynolds regimes.

2 Materials and methods

2.1 Experimental apparatus and procedures

The measurements have been carried out on an open-loop channel operated in suction, shown in figure 1. Summarizing its main features, the channel lower surface is heated by means of two Printed Circuit Boards (PCBs) independently powered and controlled. The PCBs have a substrate made of FR-4 fiberglass-reinforced epoxy laminate material, whereas copper tracks are 0.017 mm thick, 7.8 mm wide, spaced 0.2 mm apart each other, and covered by a black lacquer which also fills up the gaps between them, making the heating surface flat, smooth and with a high emissivity. A double-glazing 130 mm x 130 mm germanium window grants the optical access to a FLIR T650sc IR-camera, with a 640 x 480-pixel resolution and a 20 mK NETD at 30 °C. The main experimental features are listed in table 1. Further details on the calibration procedures for the used sensors are reported in [5].
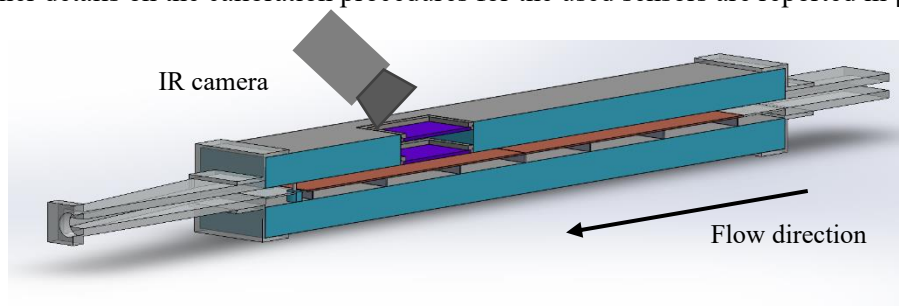

Figure 1. Lengthwise section of the test channel for local heat transfer measurements

Table 1: main geometrical parameters

H	Channel height	12	mm	L_h	Heated length	840	mm
W	Channel width	120	mm	e	Rib side dimension	4	mm
AR	Aspect ratio	10		P	rib-to-rib distance (pitch)	80	mm
D_h	Hydraulic diameter	21.8	mm	e/H	Blockage	0.33	
L	Channel length	960	mm	P/e	Adimensional pitch	20	

While the details of the experimental procedures and models are explained in details in [5] and [6], the objective of the test is to retrieve the local Nusselt number at the bottom surface, which has an imposed heat flux as boundary condition, henceforth called $Nu_{loc,q}(x,y)$ and defined as in equation 2:

$$Nu_{loc,q}(x,y) = \frac{h_{loc}(x,y)D_h}{k_{air}} \tag{2}$$

Being the hydraulic diameter D_h a constant and since the air's thermal conductivity k_{air} is considered to be so within the experimental temperature range, the uncertainties regarding $Nu_{loc,q}(x,y)$ are contained in the local convective heat transfer coefficient $h_{loc}(x,y)$, defined in equation 3 as:

$$h_{loc,q}(x,y) = \frac{q_c''(x,y)}{T_w(x,y) - T_b(x)} \tag{3}$$

Where $T_w(x,y)$ is the wall temperature, measured by IR thermography, and $T_b(x)$ the bulk fluid temperature, which is assumed to have a linear trend and therefore is determined by measuring the inlet and outlet bulk temperature, respectively named T_{in} and T_{out}.

The local convective heat flux $q_c''(x,y)$ is obtained by applying the energy balance to an element of the copper tracks of the bottom heater, i.e. where the heat generation by means of Joule's effect takes place. Considering a spanwise slice of the heater, as in figure 2, the energy balance is written as in equation 4:

$$q_c''(\bar{x},y) = \sigma_{el}s_{Cu} - q_{rad}''(\bar{x},y) - q_{k,back}''(\bar{x},y) + q_{k,y}''(\bar{x},y) - q_{k,y+dy}''(\bar{x},y) + q_{k,x}''(\bar{x},y) - q_{k,x+dx}''(\bar{x},y) \tag{4}$$
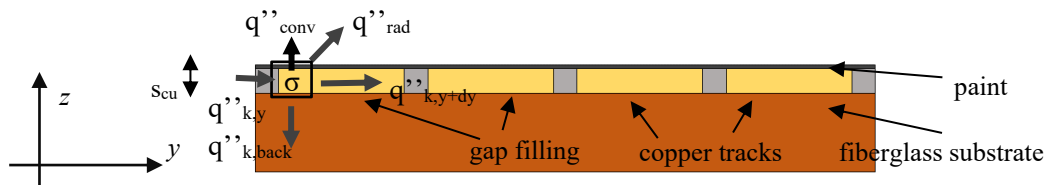
Figure 2. PCB scheme of a slice in x-y direction, with the energy balance on the copper layer

where σ_{el} is the volumetric heat dissipation by Joule effect, which is considered uniform in the copper tracks, s_{cu} the copper layer thickness, $q''_r(x,y)$ the heat flux radiated by the coating, $q''_{k,back}(x,y)$ the heat flux diffusing in the negative z direction from the rear of the copper track layer, and finally $q''_{k,y}(x,y)$ and $q''_{k,y+dy}(x,y)$ the heat fluxes transmitted by conduction in x-y direction through the layer itself. The conductive fluxes in x direction (out of plane) are also taken into account, but are not shown in Figure for clarity. The detailed description of the methods used to retrieve all the heat fluxes appearing in equation 4 can be found in [6] and is beyond the scope of this paper. Briefly, the conductive heat flux towards the backside of the breadboard is obtained by means of a 2D FEM model developed in COMSOL®, which reproduces the geometry of the channel spanwise section and calculates the heat flux using as boundary condition the measured temperature on the channel's bottom surface and the

convective and radiative heat losses towards the environment, the conductive term along the plane of the heater by applying the laplacian to the filtered temperature field, and the radiative heat flux by means of a radiative model which takes into account the presence of a double semi-transparent glazing in the IR wavelength band.

The main experimental parameters and measured temperatures of the trials presented in this paper are listed in table 2, where Q_{in} is the total power input of the heaters, which is varied as a function of Reynolds so that steady-state temperatures reached by the experimental set-up are comparable between trials and safe for the equipment.

Table 2: experimental parameters

Re	Q_{in} / W	T_{in} / °C	T_{out} / °C	$\Delta T_{in\text{-}out}$ / °C
670	11.7	25.46	35.86	10.40
800	14.2	25.50	37.19	11.69
1080	19.6	25.46	38.75	13.29
1350	24.2	25.06	38.85	13.79
2150	37.3	23.63	40.46	16.83
3200	52.7	25.93	40.89	14.96
5400	81.8	25.74	40.83	15.08
7500	115.8	26.68	42.69	16.01

2.2 Uncertainty analysis

Since the dependence of the measurand, i.e. the local heat flux, from the measurements is given by non-linear models, it is not possible to perform an uncertainty propagation as described by the first part of the GUM [11]. A Monte Carlo analysis, on the other hand, while theoretically more feasible, requires the definition of the Probability Distribution Functions for all the input quantities, which appears a feat beyond the purpose of this work. In addition to these points, also in the light of the considerations by Moffat on single-sample experiments [12], in studies like the one presented here, it can be totally misleading to provide a "certain" uncertainty value, based on uncertainties of the single measurement devices, as many uncertainty sources in complex experiments, like focus position, environmental conditions, and the positioning of the IR camera, can be easily overlooked, and the best way to validate the results is by cross-comparison with different numerical and experimental techniques applied to the same problem. Also, literature data in simple test cases can be a valuable benchmark, but is more useful to verify trends rather than exact values, which may depend on the specific experimental setup, as shown for example in figure 3 from Sun et al [13], where various trends for the heat transfer characteristics of rectangular channels are shown in a single graph.

Measurement uncertainties are due to temperature sensors, IR-camera, and mass-flow-rate meter. The standard deviation of thermocouples and thermo-resistances measurements has been evaluated by a calibration procedure in a temperature-controlled water bath, resulting in 0.02 K and 0.01 K respectively. The declared NETD of the IR camera, i.e. 0.02 K at 300 K, has been also verified in the entire measurement range, however the filtering strategy adopted can produce local temperature differences with respect to the measurement up to 1 K, with an average of 0.1 K. The effect of possible reflections is not considered in this context. The mass-flow-rate meter has been calibrated by the Italian "Istituto Nazionale di Ricerca Metrologica (INRiM)", and a 2 % accuracy is proven for the range of Reynolds numbers exploited in this research. Thermal conductivities of all test-section materials have been measured in the ThermALab laboratory with an uncertainty at most of ±4 % and radiative properties have been measured with an uncertainty of ±1 % up to 20 μm, and a constant behavior is assumed after that wavelength.
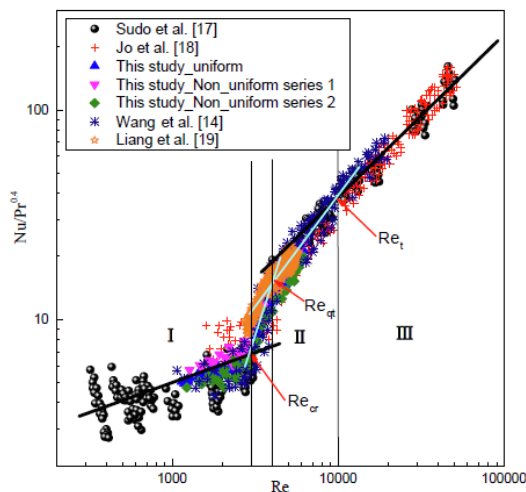
Figure 3. Experimental values of $Nu/Pr^{0.4}$ as function of Re for narrow smooth rectangular channels from Sun et al. [13], database collected from various studies carried out with different boundary conditions. They propose 2 correlations to fit data with $\pm$ 25% accuracy for laminar and transition regime and show that the Dittus-Boelter correlation has $\pm$ 20% accuracy for fully-turbulent regime (Re > 10000)

Considering this data, a minimum uncertainty on the local Nusselt number, based from the definition of equation 3, and considering only the uncertainties induced by the temperature measurements explicitly appearing in the formula, i.e. the bulk temperature $T_b(x)$ and the wall temperature $T_w(x,y)$, can be given as follows:

$$\frac{\delta Nu}{Nu} = \frac{T_w(x,y) - T_b(x)}{q_c''(x,y)} + \sqrt{\frac{q_c''(x,y)^2}{(T_w(x,y) - T_b(x))^2}\delta T_w + \frac{q_c''(x,y)^2}{(T_w(x,y) - T_b(x))^2}\delta T_b} \qquad (5)$$

The minimum average uncertainty value for the Nusselt number calculated by means of equation 5 for all configurations is equal to 12%. This value does not take into account the contribution given by the term $q_c''(x,y)$, which is affected by all the models mentioned in paragraph 2.1. As will be shown in paragraph 3, while for high-Reynolds flows $q_c''(x,y)$ can be, with good approximation, considered equal to the input heat flux, for low Reynolds other contributions have to be taken into account.

Finally, deviations from the assumed linear behaviour of $T_b(x)$, which may be caused by local radiative losses in the region of the germanium window, could introduce an estimated average bias of 5% on h, i.e. a slight underestimation, for low-Re measurements.

3   Results

Before showing the results of the tested configurations in terms of Nu/Nu_0, common trends and features of the results are analyzed for one configuration. In particular, let us consider the V-down configuration, as it is, among those tested, the one with the highest local Nu increment as the Reynolds number increases.

The first consideration regards the absolute value of the heat fluxes. Since an experimental constraint is to maintain the heated surface at an average temperature high enough to appreciate local differences induced by the convective pattern, but also to avoid overheating, the power input is set to be comparable to previous experiments in the constant-temperature channel, for each Reynolds, as in table 2. The implication of this choice is that the temperatures of the channel show very little significant variability between experiments at different Reynolds number and, consequently, all the non-convective heat fluxes have comparable absolute values. The only one that changes, along with the increasing power input at higher Reynolds, is the convective one, as shown in Figure . Figure shows the same information, but directly compares the heat flux breakdown relative to the input power for the lowest and maximum tested Re.
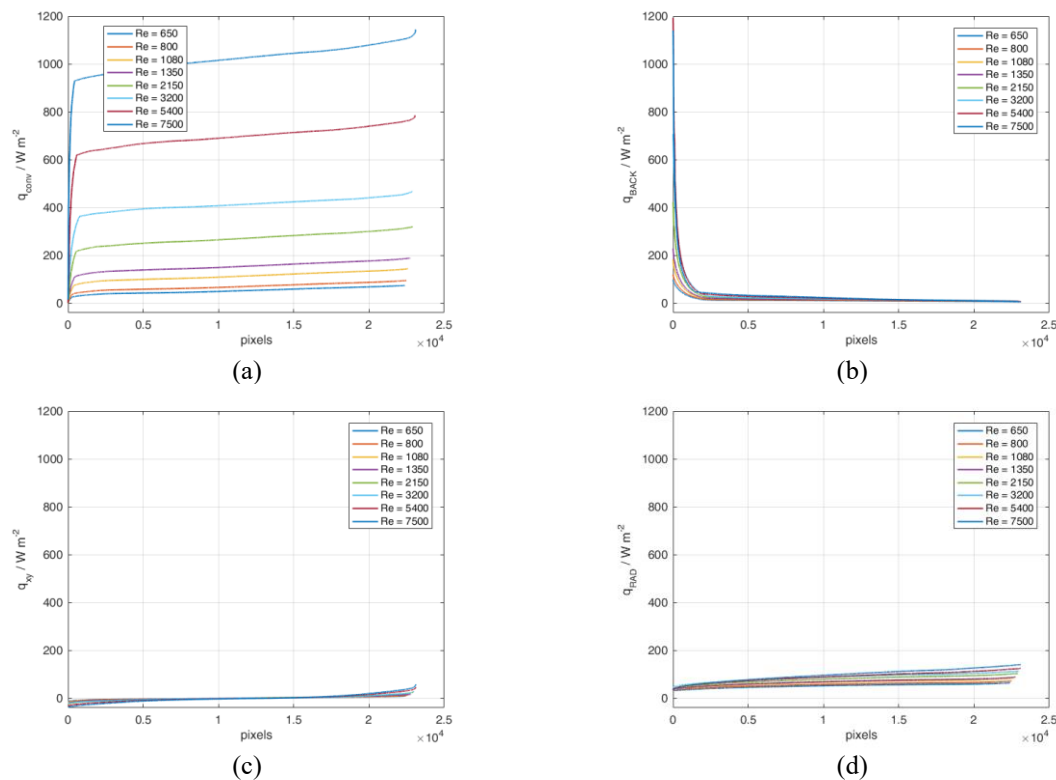
Figure 4. Heat flux maps, sorted from lowest to highest for each pixel, for each Reynolds. Convective heat flux (a), backside heat flux (b), in-plane heat flux (c) and radiative heat flux (d)
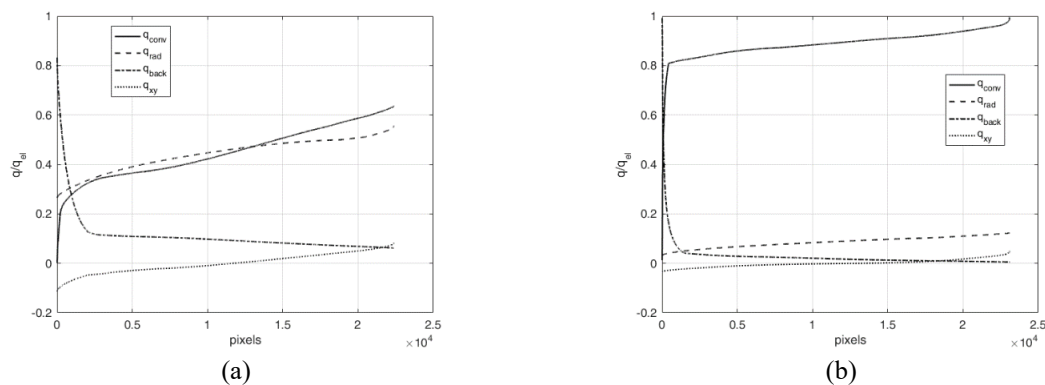

Figure 5. Sorted heat fluxes relative to the power input, Re = 670 (a) and Re = 7200 (b)

The consideration that follows is that, as the Reynolds number increases, the convective heat flux increases relatively to the other heat fluxes, with the only exception of the backside component towards the very edge, which is limited to impose a null convective flux at the corner. That implies that, as Re tends to infinity, the local convective heat flux tends to be uniformly distributed and equal to the input power. Consequently, the uncertainty on the local convective heat flux converges to that of the input power, as Reynolds number increases. Otherwise, the uncertainty linked to all the other models, in this case the radiative one, can affect the absolute measurement at lower Reynolds.

On the other hand, the local convective heat transfer coefficient $h(x,y)$ and, consequently, the local Nusselt number $Nu(x,y)$, defined by equations 2 and 3, are dependent not only on the local convective heat flux, but also on the difference between the local wall temperature $T_w(x,y)$ and the fluid bulk

temperature $T_b(x)$, which is considered linearly increasing from the inlet to outlet. In the zones of efficient heat transfer enhancement, the local wall temperature has the tendency to reach the fluid bulk temperature, thus causing a hyperbolic increment of the local heat transfer coefficient, as visible in Figure . This behavior is better seen on 2D maps, showing the percentage difference from the average heat flux and convective coefficient, as in figure 7.
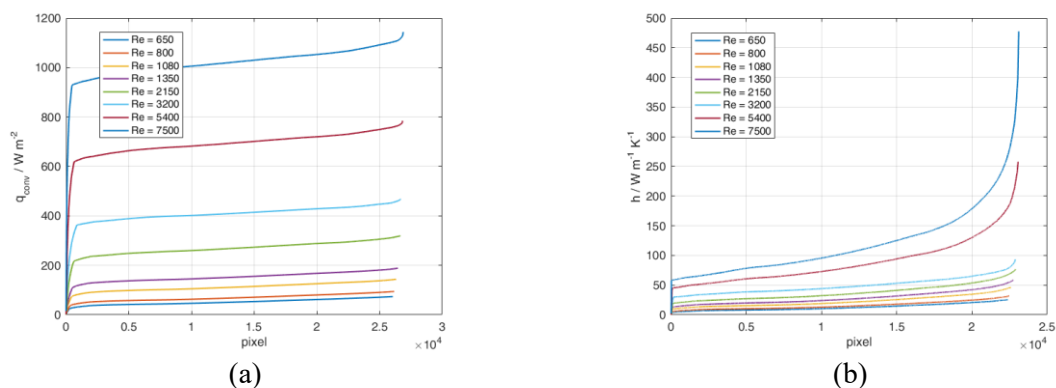

(a)   (b)

Figure 6. Sorted heat flux maps (a) and sorted local convective coefficient maps (b)
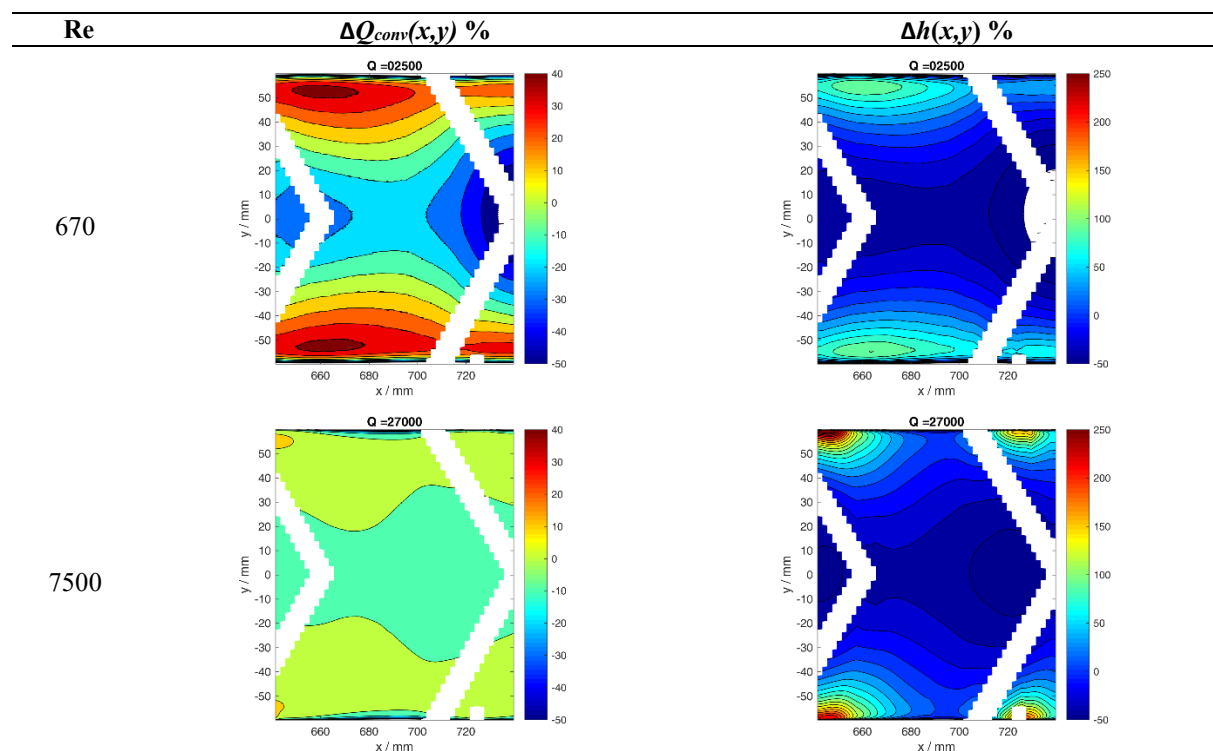

Figure 7. Maps of percentage difference from the average, convective heat fluxes (left) and convective coefficient (right), V down configuration. Q refers to the volumetric flow rate. Flow from left to right

While being partially beyond the scope of the paper, the resulting Nu/Nu$_0$ maps with respect to the smooth configuration, given by the correlations reported in [13], is shown in figure 8 for Re equal to 670, 2150 and 7500.
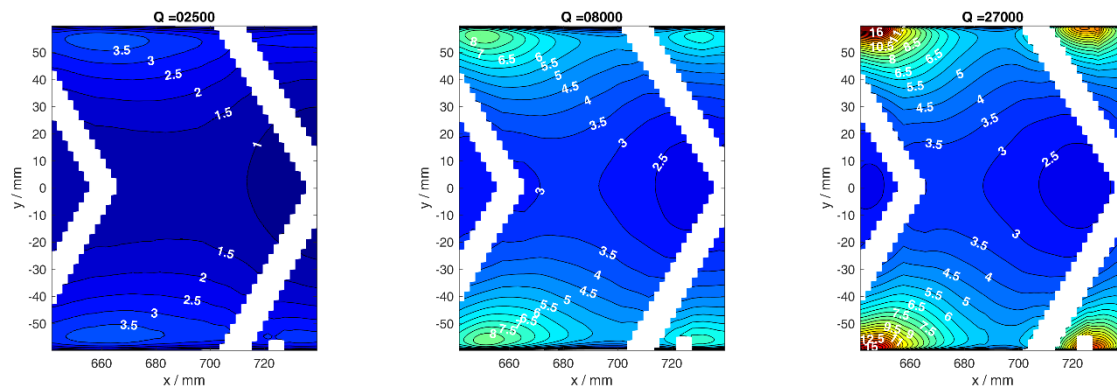
Figure 8. Nu/Nu_0 maps, for Reynolds 670, 2150 and 7500 (left to right). Flow from left to right.

4 Conclusions

This paper illustrates some considerations on the uncertainty associated with the measurement of the local heat transfer coefficient in a ribbed closed channel. In particular, the analysis shows that for high Reynolds number, i.e. Re > 10000, most of the input heat flux, for this particular experimental set-up, is transferred to the air flow by convection. As a consequence, locally, the uncertainty on the Nusselt number is mainly linked to the uncertainty of the temperature measurements, in particular to the temperature of the surface under observation and the inlet and outlet bulk temperature.

For the minimum Reynolds under investigation, i.e. Re = 650, the radiative term weighs from 40% to 60% of the heat balance, and conductive terms can account for up to 20%. The uncertainty associated with the models for their calculation can therefore be taken into account for a sounder total uncertainty definition. Finally, heat transfer increment maps for the analyzed configuration are reported, to illustrate the context of this analysis.

References

[1]   Kumar A, Kim M-H. 2015 *App. Therm. Eng.* **89** 239–61
[2]   Tanda G, Satta F 2021 *Int. J. of Heat and Mass Trans.* **169** 120906
[3]   Chung H, Park JS, Park S, Choi SM, Rhee D-H, Cho HH 2015 *Int. J. of Heat and Mass Trans.* **88** 357–67
[4]   D Fustinoni, P Gramazio, L P M Colombo and A Niro 2012 *J. Phys.: Conf. Ser.* **395** 012042
[5]   D Fustinoni, P Gramazio, L Vitali and A Niro 2017 *J. Phys.: Conf. Series* **796** 012015
[6]   P Gramazio, L Vitali, D Fustinoni and A Niro 2017 *J. Phys.: Conf. Series* **923** 012052
[7]   Gao X, Sundén B 2001 *Heat and Mass Trans.* **37** 315–20
[8]   Cavallero D, Tanda G. 2002 *Exp. Therm. and Fluid Sci.* **26** 115–21
[9]   Gupta A, SriHarsha V, Prabhu SV, Vedula RP. *Exp. Therm. and Fluid Sci.* **32** 997–1010
[10]   Peng W, Jiang P-X, Wang Y-P, Wei B-Y. 2011 *App. Therm. Eng.* **31** 2702–8.
[11]   BIPM 2010 JCGM 100:2008, Evaluation of measurement data
[12]   Moffat R J 1988 *Exp. Therm. And Fluid Sci.* **1** 3-17
[13]   Sun R, Song G, Zhang D, Deng J, Su GH, and Kulacki FA 2020 *Exp. Therm. and Fluid Sci.* **114** 110055.